

Green Chemistry

Accepted Manuscript



This article can be cited before page numbers have been issued, to do this please use: H. Zhao, Y. Jiang, P. Chen, J. Fu, X. Lu and Z. Hou, *Green Chem.*, 2018, DOI: 10.1039/C8GC01768A.



This is an Accepted Manuscript, which has been through the Royal Society of Chemistry peer review process and has been accepted for publication.

Accepted Manuscripts are published online shortly after acceptance, before technical editing, formatting and proof reading. Using this free service, authors can make their results available to the community, in citable form, before we publish the edited article. We will replace this Accepted Manuscript with the edited and formatted Advance Article as soon as it is available.

You can find more information about Accepted Manuscripts in the [author guidelines](#).

Please note that technical editing may introduce minor changes to the text and/or graphics, which may alter content. The journal's standard [Terms & Conditions](#) and the ethical guidelines, outlined in our [author and reviewer resource centre](#), still apply. In no event shall the Royal Society of Chemistry be held responsible for any errors or omissions in this Accepted Manuscript or any consequences arising from the use of any information it contains.



Green Chemistry

Paper

CoZn-ZIF derived ZnCo₂O₄-framework for the synthesis of alcohols from glycerolHuaiyuan Zhao^a, Yuanyuan Jiang^a, Ping Chen^a, Jie Fu^b, Xiuyang Lu^b, Zhaoyin Hou^{a,*}Received 00th January 2018,
Accepted 00th January 2018

DOI: 10.1039/x0xx00000x

www.rsc.org/

As a widely used solvent, fuel and intermediate, the demand of ethanol increases continuously. Currently, ethanol is produced via sugars fermentation and hydration of ethylene. It is of great significance to convert the over-supplied glycerol to ethanol. Here, we report a novel Co/ZnO catalyst with nano-sized Co particles embedded in ZnO plates that was obtained through the calcination and reduction of CoZn-ZIF precursor, and its excellent performance in the synthesis of ethanol from glycerol. The transformation process from CoZn-ZIF to Co/ZnO-ZIF was characterized by TG-DSC, XRD, SEM, TEM and XPS. Characterization results indicated that rhombic dodecahedral shaped composite consisting ZnCo₂O₄ spinel formed after calcination of CoZn-ZIF precursor, which brought the formation of small Co particles that embedded in ZnO plates during reduction. Under optimal conditions, the best yield of ethanol reached 1.45 g-ethanol/g-cat/h at 210 °C over Co/ZnO-ZIF. On the basis of a series of controlled experiments, the reaction mechanism for the formation of alcohols from glycerol was proposed.

1. Introduction

Ethanol is a widely used solvent, an intermediate of manufacturing industries and a clean fuel. The largest single use of ethanol is as an engine fuel and fuel additive. It was reported that ethanol as a fuel can reduce harmful tailpipe emissions, such as carbon monoxide, particulate matter, oxides of nitrogen and other ozone-forming pollutants.¹ And now, the use of ethanol as fuel and fuel additive is widespread all over the world, and more than 97% of gasoline in United States and Brazil contains ethanol. In last September, China planned to roll out the use of ethanol in gasoline nationally by 2020 similar to United States and Brazil, and it was predicated that the fuel ethanol production in the mainland of China will reach 4,200,000 ton in 2030.² Currently, the main resource of ethanol was the sugars fermentation and hydration of ethylene.^{3,4}

Glycerol is a by-product during the production of biodiesel, the rapidly rising production of biodiesel has led to a serious surplus of glycerol, and it was projected that the production of glycerol would be six times more than demand in 2020, which makes it become one of the most attractive platform chemicals.⁵ In the past decade, many works have been

published in order to transform glycerol to valuable products.⁶⁻¹¹

In 2015, Hutchings et al found that glycerol could directly transform into methanol over MgO.¹² In addition to methanol, ethanol was also found in their experiments. What's more, Perosa and Tundo once reported that ethanol was generated in the liquid phase hydrogenolysis of glycerol because of the cleavage of carbon-carbon bond over Ni catalyst, especially at high temperature and long reaction time.¹³ In the vapor phase hydrogenolysis of glycerol, Ryneveld et al discovered that the selectivity of methanol, ethanol and propanol increased gradually with the increasing reaction temperature over Ni/SiO₂ and Ni/Al₂O₃ catalysts.¹⁴ And several works also reported that ethanol was detected in the hydrogenolysis of glycerol.¹⁵⁻²⁰ According to these pioneering works, the selective synthesis of ethanol as a main product from the hydrogenolysis of glycerol would be possible.

Previous work in our laboratory found that Ni_{2.4}/Mg_{3.7}Cr_{2.0}O_{6.7} catalyst which derived from Ni-substituted stichtite was efficient to produce ethanol from glycerol by a "two-step hydrogenation" process, and the best yield of ethanol attained 0.50 g-ethanol/g-cat/h at 250 °C. But the formation of ethanol from glycerol was sensitive to reaction temperature, and the selectivity of ethanol decreased sharply when the reaction temperature was higher than 250 °C.²¹ At the same time, it was also confirmed that the synergic effect between Ni (hydrogenation active sites) and MgCr₂O₄ (dehydration active sites) in Ni_{2.4}/Mg_{3.7}Cr_{2.0}O_{6.7} played a crucial role in the selective formation of ethanol.

Metal-organic frameworks (MOFs) are porous materials with organic ligands and metal atoms which have special physical and chemical properties,^{22,23} and MOFs can be used as sacrificial templates to construct various porous nanostructures.^{24,25} Isomorphous MOFs was the ideal templates

^a Key Laboratory of Biomass Chemical Engineering of Ministry of Education, Department of Chemistry, Zhejiang University, Hangzhou 310028, China

^b Key Laboratory of Biomass Chemical Engineering of Ministry of Education, College of Chemical & Biochemical Engineering, Zhejiang University, Hangzhou 310027, China.

† Footnotes relating to the title and/or authors should appear here.

Electronic Supplementary Information (ESI) available: [preparation procedures, SEM images of reference catalysts, XRD and XPS of reduced catalysts, product distribution of different starting materials over Co/ZnO-ZIF]. See DOI: 10.1039/x0xx00000x

to build heterogeneous composite with controlled composition and interaction between individual components.²⁶ In this work, nano Co particles that embedded in ZnO plates were synthesized through the controlled calcination and reduction of CoZn-ZIF ($[M(\text{CH}_3\text{C}_3\text{H}_2\text{N}_2)_2]_n$, M=Co and Zn) precursor and used in the continuous hydrogenolysis of glycerol to ethanol. It was found that this special structured Co/ZnO-ZIF catalyst exhibited predominant activity and selectivity for the formation of ethanol at lower temperature (210 °C) among those tested Co/ZnO catalysts that prepared via co-precipitation, impregnation and solvent-free grinding.

2. Experimental

2.1. Catalyst preparation

CoZn-ZIF was synthesized according to the procedure that reported in reference.²⁷ In a typical process, $\text{Co}(\text{NO}_3)_2 \cdot 6\text{H}_2\text{O}$ and $\text{Zn}(\text{NO}_3)_2 \cdot 6\text{H}_2\text{O}$ (molar ratio of Co/Zn = 1/1, total metal ion molar was 15 mmol) were dissolved in methanol (75 mL) to form a clear solution. And then, the methanol solution of 2-methylimidazole (2-Melm) (75 mL, including 120 mmol 2-Melm) was added slowly into above solution. After vigorously stirring for 2 h, the mixture was incubated at room temperature for 24 h. The as-obtained precipitation was centrifuged, washed with methanol for several times, and dried at 60 °C overnight in vacuum. For convenience, the as-prepared precursor was denoted as CoZn-ZIF.

Subsequently, the as-prepared CoZn-ZIF precursor was heated to 400 °C and calcined at 400 °C in a flow of air for 3 h. The calcined product was denoted as CoZnO-ZIF. Finally, the calcined CoZnO-ZIF was further reduced in hydrogen flow (80 mL/min) at 450 °C for 1 h before the catalytic reaction, and these reduced catalysts were denoted as Co/ZnO-ZIF. The bulk composition of calcination sample was determined by inductively coupled plasma-atomic emission spectroscopy (ICP-AES; Thermo Elemental IRIS Intrepid), and these data were summarized in Table 1.

As references, several Co/ZnO catalysts with similar composition were prepared in the traditional co-precipitation (denoted as Co/ZnO-CP), impregnation (denoted as Co/ZnO-IM) and solvent-free grinding²⁸ (denoted as Co/ZnO-SF). The preparation procedures of these catalysts were described in detail in the supplementary information section. These catalysts were also calcined and reduced under the same conditions as that of Co/ZnO-ZIF.

2.2. Characterizations

Powder X-ray diffraction (XRD) patterns of precursor, calcined catalysts and reduced catalysts were collected on a Rigaku D/WAX-2500 diffractometer which uses $\text{Cu K}\alpha$ radiation (1.5406 Å) with a step of 0.02° and 5°/min from 5 to 80° at room temperature. Scanning electron microscope (SEM) images were detected on Leo Evo Series SEM (VP 1430, Germany) at an accelerating voltage of 3 kV. Platinum was used to coat samples in order to avoid charging. N_2 adsorption was tested at its normal boiling point using an ASAP 2010 analyzer (Micromeritics) after pretreated at 150 °C for 4 h in vacuum. Brunner-Emmet-Teller (BET) method was used to calculate specific surface area ($P/P_0 = 0.0-0.01$ for MOFs and 0.05-0.3 for other samples) and the Horvath-

Kawazoe (HK) method was used to calculate pore size distributions from 0-2 nm and the Barrett-Joyner-Halenda (BJH) method was used for pore size larger than 2 nm. Thermogravimetric and differential scanning calorimeter (TG-DSC) analysis was carried out on a Netzsch STA 409 thermobalance. Analysis was measured from 25 to 700 °C at a heating rate of 10 °C /min in air flow (30 mL/min). Transmission electron microscope (TEM) images were gotten by using an accelerating voltage of 200 kV (JEOL-2020 F). Elemental mapping was performed with FEI TECNAI F30 microscope operated at 300 kV. X-ray photoelectron spectroscopy (XPS) measurements were carried out on a Kratos Axis Ultra DLD system with a base pressure of 10^{-9} Torr.

Temperature-programmed reduction (H_2 -TPR) of all catalysts was carried out in the following process: 50 mg sample was first pretreated at 500 °C for 1 h in Ar flow (30 mL/min) and then cooled to room temperature. Finally, a reduction gas (10% H_2 /Ar mixture, 30 mL/min) was shifted and the reactor was heated to 700 °C at a heating rate of 15 °C /min. Powder KOH was used to dry effluent and the amount of hydrogen H_2 ($m/e = 2$) consumption was detected and recorded by a quadrupole mass spectrometer (OmniStar™, GSD301, Switzerland).

2.3. Catalytic reaction

Hydrogenolysis of glycerol was performed in a vertical fixed-bed reactor and a back pressure regulator was used to control the system pressure. The reactor was a stainless steel tube and the internal diameter was 6 mm, the length was 540 mm. In a typical run, 0.10 g catalyst (40-60 mesh) was charged in the constant temperature part of the reactor and quartz sand was packed in both ends. Before reaction, catalyst was in situ reduced in pure H_2 flow (80 mL/min) at 450 °C for 1 h. Subsequently, the reactor was cooled to scheduled reaction temperature and pressure adjusted to 2.0 MPa. 40 wt% of glycerol aqueous solution was fed into the reactor continuously at a flow rate of 0.02 mL/min. The reaction products and unreacted glycerol were cooled in a condenser (remained at 0 °C) and collected in a gas-liquid separator, weighed and analyzed on a gas chromatograph (Shimadzu, 14B) which was equipped with a FID and a 30-m capillary column (DB-WAX 52 CB, USA). All products detected in the liquid were verified by a gas chromatography-mass spectrometry system (GC-MS, Agilent 6890) and quantified through an external calibration method. Methane, CO and CO_2 in gas phase were analyzed in an on-line gas chromatograph (Shimadzu, 8A) equipped with TCD detector. Every analysis was carried out after a steady operation for 2 h, and the carbon balance was calculated in all experiments.

3. Results and discussion

3.1. The structure of CoZn-ZIF precursor

Powder XRD analysis confirmed that the prepared CoZn-ZIF precursor exhibited the same diffraction pattern with original ZIF-8 ($[\text{Zn}(2\text{-Melm})_2]_n$, JCPDS 00-062-1030) (Fig. 1A), which indicated the homogenous substitution of Co and Zn due to their similar ionic radius and electronegativity.²⁹ The SEM image (Fig. 1B) showed clearly that the synthesized CoZn-ZIF crystals had a rhombic dodecahedral outline.

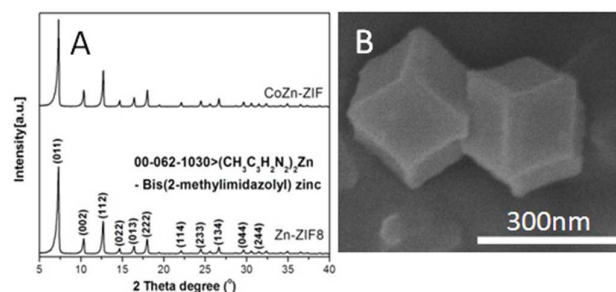


Fig. 1 XRD pattern (A) and SEM image (B) of CoZn-ZIF precursor.

N_2 sorption isotherm of fresh CoZn-ZIF was type I model and there was a rapid rise of N_2 uptake at 0–0.01 of P/P_0 (Fig. 2), which was the feature of microporous material. The calculated BET surface area and pore volume of CoZn-ZIF were $1528 \text{ m}^2/\text{g}$ and $0.64 \text{ cm}^3/\text{g}$, respectively. These data indicated that the synthesized CoZn-ZIF had a well-distributed microporous channels at 0.67 nm and there were some pores with the diameter of 0.99 nm, which was similar to the previous report.³⁰

3.2. Synthesis of Co/ZnO-ZIF from CoZn-ZIF

The thermal stability of fresh CoZn-ZIF precursor was detected via TG-DSC analysis (Fig. 3A). It was found that there were two major weight losses during the calcination of CoZn-ZIF, the first weight loss at 20–300 °C was attributed to the volatilization of water and methanol in the pores of CoZn-ZIF, and the second loss at 300–470 °C with a strong exothermal signal was the combustion of (2-Melm)⁺. The weight of sample was no obvious change in the following calcination process. The weight loss of CoZn-ZIF between 300 and 470 °C was 57.1%, which was consistent with the chemical compositions of $M(2\text{-Melm})_2$ ($M=\text{Co}$ and Zn) transforming into metal oxide. In order to obtain the nanobox structure, the thermal decomposition temperature was determined as 400 °C. In this temperature, the ligand (2-Melm)⁺ was decomposed slowly and the rhombic dodecahedron morphology could be retained. Fig. 3B showed the XRD patterns of calcined CoZn-ZIF and those reference catalysts prepared in different methods. It

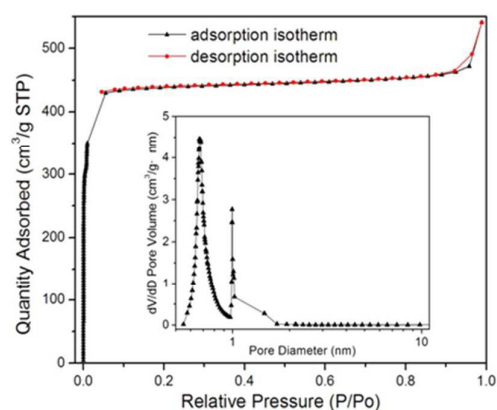


Fig. 2 N_2 adsorption-desorption isotherm and pore volume distribution (insert) of CoZn-ZIF.

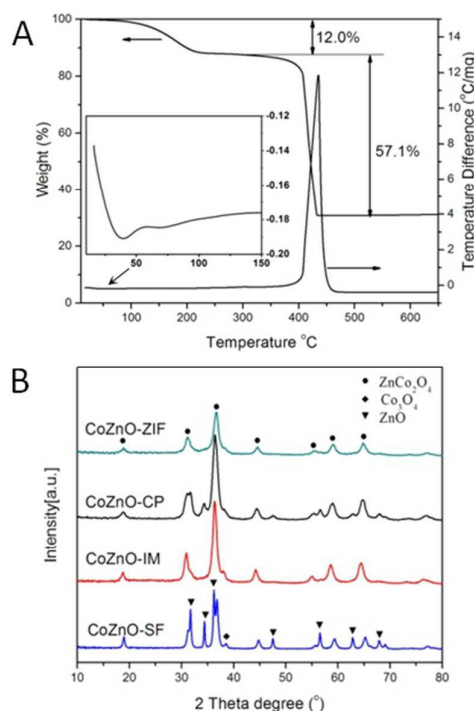


Fig. 3 TG and DSC curve (A) of CoZn-ZIF precursors under air atmosphere; XRD patterns (B) of CoZnO-ZIF, CoZnO-CP, CoZnO-IM and CoZnO-SF.

could be found that original structure of CoZn-ZIF precursor collapsed and mainly spinel ZnCo_2O_4 (JCPDS 00-023-1390) formed in the calcined CoZnO-ZIF. But in those reference catalysts prepared via co-precipitation (CoZnO-CP), impregnation (CoZnO-IM) and solvent-free grinding (CoZnO-SF), separated ZnO (JCPDS 01-079-5604) and Co_3O_4 (JCPDS 00-043-1003) were also detected besides ZnCo_2O_4 . These results indicated that the homogeneously dispersed cobalt/zinc ions in the framework of CoZn-ZIF precursor were more favorable for the formation spinel structured ZnCo_2O_4 , in which cobalt/zinc ions remained their atomic dispersion.

SEM images and TEM images (Fig. 4A-D) further disclosed that the CoZn-ZIF derived sample still remained their original rhombic dodecahedral shape. But the faces of calcined CoZnO-ZIF became concave and rough, the edge was prominent because of the decomposition of organic ligand and the oxidation of cobalt/zinc ions.³¹ The corresponding elemental mapping revealed that Co and Zn were uniformly distributed in the rhombic dodecahedral composite (Fig. 4E) and the corresponding spectra was showed in Fig. S1. High-resolution TEM image at the edge of these composite (Fig. 4F) clearly showed that those spinel ZnCo_2O_4 particles stacked tightly and the exposed crystal faces were different seeing from the lattice fringe. That is, CoZnO-ZIF was a porous and hollow structure which was built by spinel ZnCo_2O_4 particles. The SEM images of reference catalysts were illustrated in Fig. S2 of the supporting information.

N_2 adsorption analysis also disclosed that the calcined CoZnO-ZIF was a porous and hollow architecture with highest surface area and bigger pore volume among those reference catalysts prepared in different methods (see Table 1 and Fig. 5).

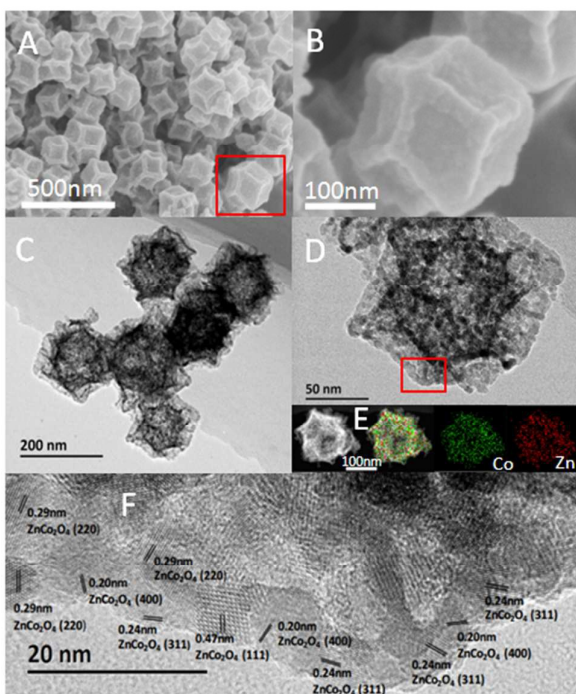


Fig. 4 SEM (A,B) and TEM images (C,D,F) of CoZnO-ZIF; element mapping of an individual nanobox (E).

It was found that CoZnO-ZIF showed a typical type IV adsorption isotherm and a H3-type hysteresis loop at a relative pressure of 0.45–1.0. The calculated BET surface area and pore

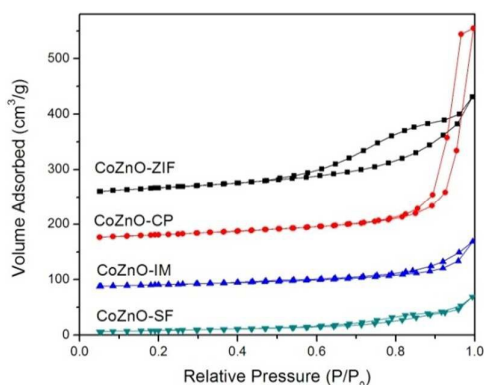


Fig. 5 N₂ adsorption–desorption isotherms of CoZnO-ZIF, CoZnO-CP, CoZnO-IM and CoZnO-SF.

volume of CoZnO-ZIF reached 97.7 m²/g and 0.30 cm³/g, respectively. While CoZnO-CP, CoZnO-IM and CoZnO-SF had a type I adsorption isotherm, and their surface area decreased to 74.2, 39.7 and 30.2 m²/g, respectively.

The H₂-TPR profiles of CoZnO-ZIF and those reference catalysts were shown in Fig. 6. It could be found that there were mainly two reduction peaks detected in all the samples. The initial reduction temperature (260 °C) and the center temperature of the first peak (330 °C) were similar in all samples, but the outline and the center temperature of the second peak varied obviously. The calculated ratios of hydrogen consumption of these two peaks in CoZnO-ZIF, CoZnO-CP, CoZnO-IM and CoZnO-SF were 2.1, 2.6, 2.4 and 2.9, respectively. According to above characterization results and published works,^{32–34} the first hydrogen consumption peak could be ascribed to the reduction of Co³⁺ in ZnCo₂O₄ (in CoZn-ZIF) and/or mixed ZnCo₂O₄+Co₃O₄ (in reference catalysts) to Co²⁺, and the second hydrogen consumption peak was the reduction of Co²⁺ to Co⁰. The calculated ratio of hydrogen consumption (2.1) and the successive reduction profile of CoZnO-ZIF also indicated that mainly ZnCo₂O₄ formed. These results fitted well with above XRD analysis.

The binding energy of Co 2p_{3/2} in CoZnO-ZIF, CoZnO-CP, CoZnO-IM and CoZnO-SF was shown in Fig. 7A. The spectra of Co 2p_{3/2} were deconvoluted into two peaks at 780.2 and 781.3 eV, which could be assigned to that of Co²⁺ and Co³⁺.^{35,36} These results further indicated that mainly spinel ZnCo₂O₄ formed in CoZnO-ZIF, while both Co₃O₄ and spinel ZnCo₂O₄ coexisted in those reference samples. At the same time, the asymmetric spectra of O1s in these samples could be deconvoluted into three peaks centered at 529.3, 530.4 and 531.5 eV, which were attributed to the oxygen in Co₃O₄,³⁷ ZnCo₂O₄³⁸ and ZnO,³⁹ respectively (Fig. 7B). These results were

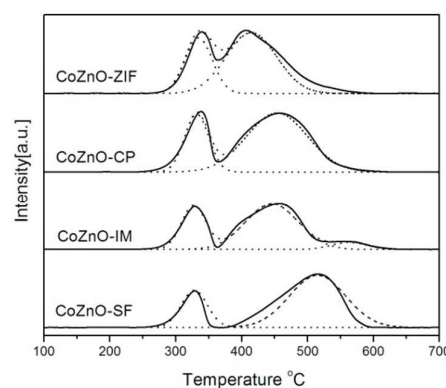


Fig. 6 H₂-TPR profiles of CoZnO-ZIF, CoZnO-CP, CoZnO-IM and CoZnO-SF.

Table 1. The composition and textural properties of CoZnO.

Sample	Co:Zn composition ^a (molar ratio)	Surface Area (m ² /g)	Pore Volume (cm ³ /g)	Pore diameter (nm)
CoZnO-ZIF	1.1 : 1	97.7	0.30	8.9
CoZnO-CP	1.0 : 1	74.2	0.61	26.2
CoZnO-IM	0.9 : 1	39.7	0.14	12.5
CoZnO-SF	1.0 : 1	30.2	0.11	12.1

^a Calculated from ICP analysis.

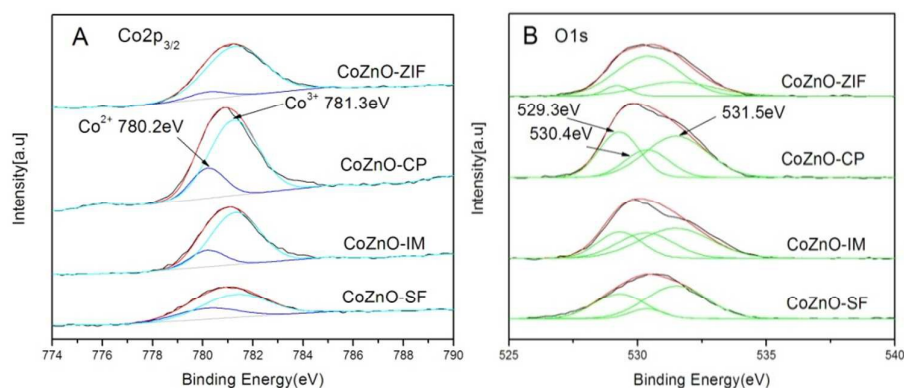


Fig. 7 The binding energy of Co $2p_{3/2}$ (A) and O 1s (B) in CoZnO samples.

consistent with above characterizations, which further confirmed that mainly $ZnCo_2O_4$ formed in the process of CoZn-ZIF calcination under air flow.

3.3. The properties of Co/ZnO

XRD (Fig. S3) and XPS (Fig. S4) analysis of the reduced catalysts confirmed that both spinel $ZnCo_2O_4$ and Co_3O_4 could be reduced in hydrogen flow at $450\text{ }^\circ\text{C}$ for 1 h. Metallic Co (JCPDS 01-023-4651) and ZnO (JCPDS 01-079-5604) were detected in these reduced samples. According to the half-width of Co (111), the calculated crystallite size of Co NPs in reduced Co/ZnO-ZIF, Co/ZnO-CP, Co/ZnO-IM and Co/ZnO-SF was 10.3, 15.8, 14.8 and 23.9 nm,

respectively. These data indicated that spinel $ZnCo_2O_4$ intermediate was favorable for the formation of highly dispersed Co particles.

The surface composition of these samples before and after reduction was analyzed via XPS and summarized in Table 2. It was found that the detected mole ratio of surface Co/Zn increased from 1.12 (in CoZnO-ZIF, before reduction) to 1.42 (in Co/ZnO-ZIF, after reduction), which meant that Co dispersed mainly on the surface of reduced Co/ZnO-ZIF, and/or the particle size of Co was small. On the other hand, the mole ratio of Co/Zn decreased sharply from 0.83 (in CoZnO-SF, before reduction) to 0.42 (in Co/ZnO-SF, after reduction), which inferred that partial Co would be covered by Zn and/or the particle size of Co enlarged after reduction.

Table 2. Surface composition of catalysts before and after reduction.^a

Catalyst	Surface composition (mole ratio)					
	Before reduction			After reduction		
	Co	Zn	Co/Zn	Co	Zn	Co/Zn
CoZnO-ZIF	23.6	21.1	1.12	41.5	29.2	1.42
CoZnO-CP	22.6	25.1	0.90	28.0	36.0	0.78
CoZnO-IM	21.1	25.7	0.82	30.3	34.8	0.87
CoZnO-SF	22.4	27.0	0.83	17.3	41.3	0.42

^a Calculated from survey scan results of XPS.

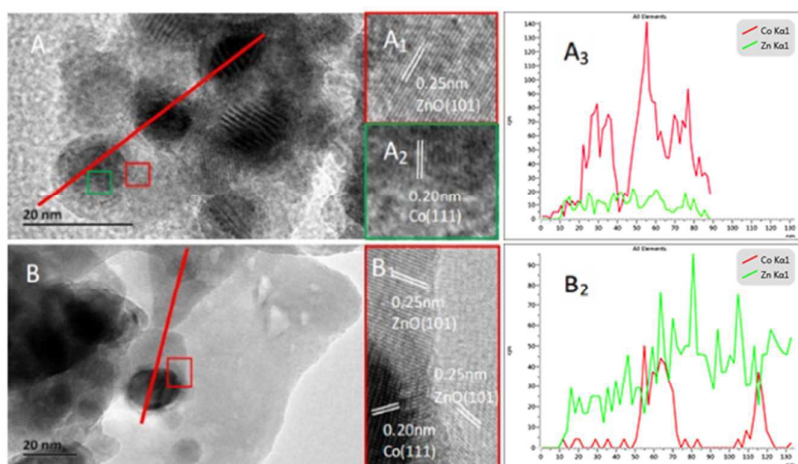


Fig. 8 TEM images of Co/ZnO-ZIF (A, A₁, A₂) and Co/ZnO-SF (B, B₁); Line-EDS of Co/ZnO-ZIF (A₃) and Co/ZnO-SF (B₂).

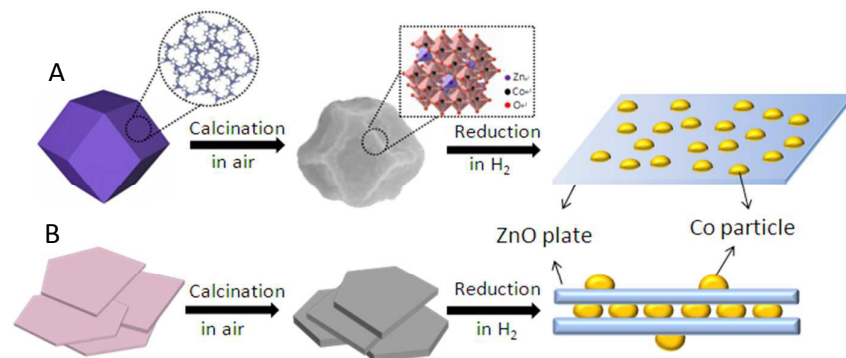


Fig. 9 Schematic diagram of prepared Co/ZnO-ZIF (A) and Co/ZnO-SF (B).

The surface enriched and small sized Co particles in reduced Cu/ZnO-ZIF were clearly identified in its high resolution TEM images (Fig. 8A) and corresponding Line-scan EDS analysis (Fig. 8A₃). Both the lattice fringes ascribed to ZnO (see Fig. 8A₁, in red square), Co (see Fig. 8A₂, in green square) and Line-scan EDS analysis confirmed that small Co NPs were embedded in the surface of thin ZnO plate. On the other hand, HRTEM analysis (Fig. 8B and 8B₁) and corresponding Line-scan EDS analysis (Fig. 8B₂) also confirmed that Co particles in reduced Cu/ZnO-SF were completely sandwiched between ZnO plates and partial surface of Co particles was covered with thick ZnO. On the basis of above results, the proposed structure of reduced Cu/ZnO-ZIF and Cu/ZnO-SF was depicted in Fig. 9A and Fig. 9B, respectively.

3.4. Synthesis alcohols over Co/ZnO catalysts prepared in different methods

Table 3 summarized the results of Co/ZnO catalysts that synthesized in different methods (with the same weight) for the continuous hydrogenolysis of glycerol in a vertical fixed-bed reactor at 210 °C, 2.0 MPa. It was found that Co/ZnO-ZIF showed an outstanding performance, the detected conversion of glycerol reached up to 98.8% with a 57.9% selectivity of ethanol and a 94.2% selectivity of mono alcohol (including methanol, ethanol, 1-PO and 2-PO). Among those reference catalysts, the conversion of glycerol over Co/ZnO-CP and Co/ZnO-IM exceeded 96%, but the selectivity of ethanol decreased to 33.7 and 37.1%, respectively. On the other hand, mainly 1,2-PDO formed over Co/ZnO-SF and the selectivity of ethanol decreased sharply to 6.0% under the same condition.

Those controlled experiments with equivalent catalyst surface areas presented in the reactor also confirmed that Co/ZnO-ZIF was

the most active and selective one for the formation ethanol (see Table S1).

These results indicated that the performance of Co/ZnO catalysts for the hydrogenolysis of glycerol depended strongly on its structure. Above characterizations indicated that small sized Co particles were enriched on the surface of thin ZnO plate during the reduction of Co/ZnO-ZIF (see Table 2, Fig. 8). And this special structure (Co NPs embedded in ZnO plate, see Fig. 9A) enhanced the accessibility of glycerol and hydrogen to the surface of Co, which accelerated the hydrogenolysis of glycerol.^{19,40} On the contrary, the lowest activity of Co/ZnO-SF could be attributed to that Co particles were sandwiched between ZnO plates and partial surface of Co was covered by ZnO (see Fig. 9B).

3.5. Synthesis alcohols over Co/ZnO-ZIF under varied conditions

The performance of Co/ZnO-ZIF for the synthesis of alcohols under varied reaction temperature (190 to 250 °C) was shown in Fig. 10. It was found that the conversion of glycerol reached 92.7% at 190 °C, and mainly 1,2-PDO was detected in the reaction mixture (the selectivity of 1,2-PDO was 41.2%). The selectivity of ethanol increased quickly from 21.9 (at 190 °C) to 57.9% (at 210 °C) with the increasing temperature, and then decreased slightly under higher temperature (>220 °C) with a complete conversion of glycerol. Similar tendency was also detected over Co/ZnO-CP, Co/ZnO-IM and Co/ZnO-SF catalysts, but the selectivity of ethanol passed its maximum at 250, 230 and 250 °C, respectively (see Fig.S5). These results indicated that high temperature was more favourable for the hydrogenation and the cleavage of C-C and C-O.¹⁴ Thus, an appropriate reaction temperature was necessary for the selective hydrogenolysis of glycerol to ethanol.

Table 3. The performance of Co/ZnO catalysts for hydrogenolysis of glycerol.

Catalyst	Conversion (%)	Production selectivity in liquid phase (%)				Carbon balance (%) ^b
		1,2-PDO	Ethanol	PO	Others ^a	
Co/ZnO-ZIF	98.8	4.8	57.9	36.0	1.3	93.5
Co/ZnO-CP	96.8	28.2	33.7	27.1	11.0	95.1
Co/ZnO-IM	97.7	26.3	37.1	24.7	11.9	94.6
Co/ZnO-SF	73.6	66.7	6.0	6.6	20.7	98.2

Reaction conditions: catalyst, 0.10 g; 2.0 MPa, 210 °C; 40 wt.% of glycerol aqueous solution 0.02 mL/min, and H₂/glycerol = 40 (mol) in feed; data acquisition after steady operation for 2h.

^aIncluding methanol, ethylene glycol, acrolein, acetol and acetaldehyde etc. ^b(All carbon atoms detected in liquid products)/(All carbon atoms in feed) × 100%.

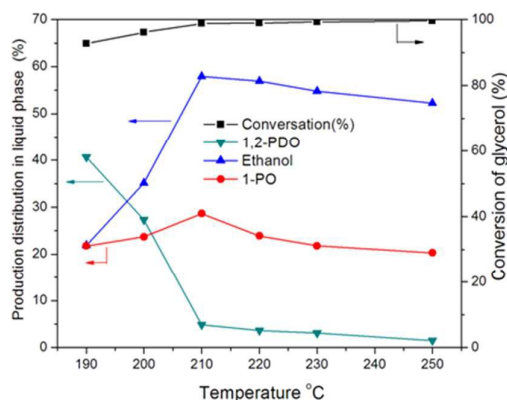


Fig. 10 Hydrogenolysis of glycerol at varied temperature over Co/ZnO-ZIF. Reaction conditions: catalyst 0.10 g; 2.0 MPa; 40 wt.% of glycerol aqueous solution, 0.02 mL/min, and H_2 /glycerol = 40 (mol) in feed; data acquisition after steady operation for 2h.

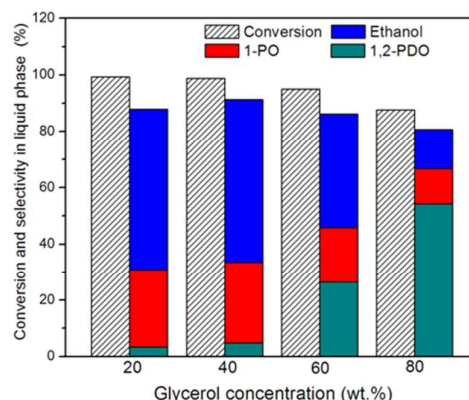


Fig. 11 Hydrogenolysis of glycerol with varied concentration of glycerol in feed over Co/ZnO-ZIF.

Reaction conditions: catalyst 0.10 g; 2.0 MPa, 210 °C; glycerol aqueous solution, 0.02 mL/min, and H_2 /glycerol = 40 (mol) in feed; data acquisition after steady operation for 2h.

Fig. 11 showed the performance of Co/ZnO-ZIF for the hydrogenolysis of glycerol with different concentration of glycerol in feed. It was found that the conversion of glycerol decreased slightly from 99.3 to 87.7% when the concentration of glycerol in feed was increased from 20 to 80 wt.%. The selectivity of ethanol and 1-PO decreased severely with the increasing concentration of glycerol, and mainly 1,2-PDO formed when using 80 wt.% glycerol as feedstock. These results might be attributed to the fact that high viscosity of glycerol would bring mass transfer limitations⁴¹ and the consecutive hydrogenolysis of 1,2-PDO to ethanol was retarded. In this case, 40 wt.% aqueous solution of glycerol was optimal and the best yield of ethanol reached 1.45 g-ethanol/g-cat/h.

Hydrogenolysis of glycerol over Co/ZnO-ZIF under different hydrogen pressure indicated that the conversion of glycerol was less sensitive to hydrogen pressure (see Fig. S6). But the selectivity of ethanol increased quickly from 29.1 (at 0.5 MPa) to 57.9% (at 2.0 MPa) with the increasing pressure at first, and then decreased slightly at higher hydrogen pressure (>2.5 MPa). The selectivity of 1,2-PDO decreased continuously from 28.2 to 4.1% with the increasing selectivity of 1-PDO (from 19.6 to 34.6%) in the tested 0.5-3.0 MPa.

The molar ratio of H_2 /glycerol in feed also exhibited significant influence on the production distribution during the hydrogenolysis of glycerol over Co/ZnO-ZIF (see Fig.S7). It was found that the conversion of glycerol exceeded 93% in all experiments. The selectivity of ethanol increased quickly from 12.7 to 58.1% with the increasing ratio of hydrogen in feed, and the selectivity of 1-PO also increased steadily from 10.2 to 29.5%. On the other hand, the selectivity of 1,2-PDO decreased from 59.2 to 3.9%. These results indicated high flow H_2 , as a carrier gas, could transfer reactants and products timely, which was beneficial to the glycerol hydrogenolysis. At the same time, that large amount of H_2 could speed up the deep hydrogenation.¹⁵

3.6. Possible mechanism of glycerol hydrogenolysis over Co/ZnO-ZIF

Fig. 12 exhibited the performance of Co/ZnO-ZIF for hydrogenolysis of glycerol under different weight hourly space

velocity (WHSV) at 210 °C and 2.0 MPa. It was found that (1) the conversion of glycerol increased quickly from 24.9% (at 0.015 h) to 98.8% (at 0.076 h) and then remained higher than 99%. (2) Acetol was the first intermediate during the hydrogenolysis of glycerol and it transformed rapidly. The detected selectivity of acetol decreased sharply from 47.8% (at a 24.9% conversion of glycerol) to 1.6% (at a 95.4% conversion of glycerol). (3) The detected selectivity of 1,2-PDO and EG went up with the conversion of glycerol at first, reached their maximum (63.0% and 16.2%, at a 74.3% conversion of glycerol) and then decreased. (4) The selectivity of ethanol and 1-PO increased continuously along with the conversion of glycerol and reached their maximum (57.9% and 28.6%, respectively) at a 98.8% conversion of glycerol. After that, the selectivity of ethanol and 1-PO decreased slightly with the increasing contact time, which could be attributed to that it would be the further decompose of ethanol and 1-PO to methanol, CO, CH_4 and/or CO_2 . The best yield of

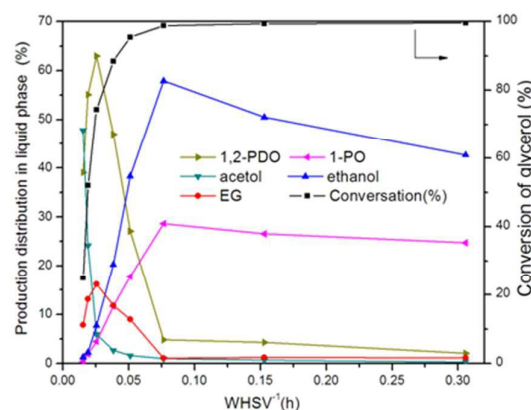


Fig. 12 Hydrogenolysis of glycerol over Co/ZnO-ZIF at various WHSV. Reaction conditions: catalyst, 0.10 g; 2.0 MPa; 210 °C; 40 wt% of glycerol aqueous solution with the feed of 0.005-0.1 mL/min, and H_2 /glycerol = 40 (mol) in feed; data acquisition after steady operation for 2 h. WHSV (weight hourly space velocity) = mass of aqueous feed solution/hour/mass of catalyst.

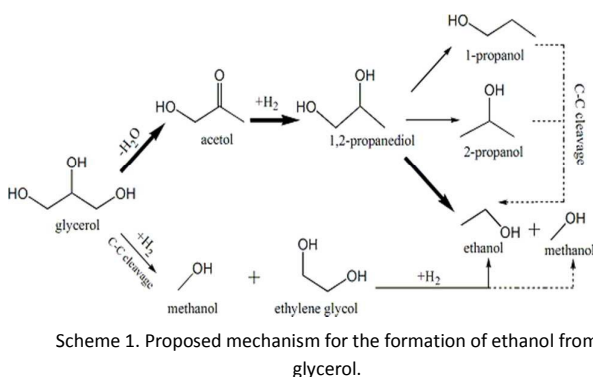
ethanol reached 1.45 g-ethanol/g-cat/h. The performance of Co/ZnO-SF under various WHSV was showed in Fig. S8 and it was found that the product distribution changed in similar tendency. And the calculated product distribution under iso-conversion level of glycerol over Co/ZnO-ZIF and Co/ZnO-SF were summarized and compared in Table S2. Table S3 summarized the product distribution under iso-conversion level of glycerol over different catalysts at different temperature. It was found that the selectivity of detected products over these catalysts was similar.

At the same time, a series of controlled experiments, in which 1,2-PDO, EG, 1-PO, 2-PO and ethanol were used as the starting materials, were carried out in order to explore reaction mechanism of ethanol synthesis from glycerol over Co/ZnO-ZIF. The results of these experiments were summarized in Table S4. It was found that (1) when 1,2-PDO was used as the starting material, the product distribution was similar with that of glycerol. (2) Mainly ethanol formed in the consecutive hydrogenolysis of EG. (3) 1-PO and 2-PO could be further hydrogenated to ethanol due the cleavage of C-C bond, but the detected conversion was quite low. (4) Under the reaction condition, ethanol (in feed) was relative stable compared with glycerol, 1,2-PDO and EG.

On the basis of the above results and the mechanism previously proposed in literatures,^{14,21,42,43} we thought that mechanism for ethanol synthesis from glycerol could be depicted in the following Scheme 1. Acetol was the direct dehydration production of glycerol, and then it converted to 1,2-PDO quickly via hydrogenation on the surface of Co/ZnO-ZIF. 1,2-PDO could be consecutively hydrogenated to ethanol, 1-PO, 2-PO and methanol. At the same time, a parallel reaction from glycerol would also occur simultaneously, in which EG formed directly from the cracking of glycerol, and EG could be hydrogenated to ethanol. Controlled experiments over Co/ZnO-ZIF further indicated that ethanol was relative stable under the reaction condition (see Table S4).

4. Conclusion

In summary, we found that a novel structured Co/ZnO catalyst could be synthesized via the controlled pyrolysis and reduction of CoZn-ZIF precursor and it showed the best performance for the continuous hydrogenolysis of glycerol in a fixed-bed reactor comparing with Co/ZnO catalysts prepared by co-precipitation, impregnation and solvent-free grinding. Characterization indicated that the mainly spinel ZnCo₂O₄ formed in calcined CoZnO-ZIF, and the initial rhombic dodecahedral structure with high surface area and big pore volume remained. Highly dispersed Co NPs that embedded in thin ZnO plates formed during the reduction of



CoZnO-ZIF. The best selectivity of ethanol over Co/ZnO-ZIF catalyst reached 57.9% (the yield of ethanol reached 1.45 g-ethanol/g-cat/h) at 210 °C, and ethanol was relative stable under the reaction condition. Those controlled experiments with varied weight hourly space velocity, different starting materials and other experiments suggested that ethanol formed mainly via the consecutively hydrogenation of glycerol (via 1,2-PDO intermediate). At the same time, a parallel routine via the cracking (of glycerol to EG) and hydrogenation (of EG) also occurred on Co/ZnO-ZIF.

Conflicts of interest

There are no conflicts to declare.

Acknowledgements

This work was financially supported by the National Natural Science Foundation of China (Contract Nos. 21773206, 21473155, 21273198) and Natural Science Foundation of Zhejiang Province (Contract No. LZ12B03001).

References

- G.A. Mills, E.E. Ecklund, *Annu. Rev. Energ. Env.*, 2003, **12**, 47-80.
- R. He, Z. Zhao, P. Liu, Z. Li, *ACS Sustain. Chem. Eng.*, 2018, **6**, 4633-4647.
- C.A. García, F. Manzini, J.M. Islas, *Renew. Sust. Energ. Rev.*, 2017, **72**, 1199-1207.
- M. Karimi, B. Jenkins, P. Stroeve, *Renew. Sust. Energ. Rev.*, 2014, **40**, 400-421.
- J.J. Bozell, *Science*, 2010, **329** 522-523.
- P. Gallezot, *Chem. Soc. Rev.*, 2012, **43** 1538-1558.
- C.H. Zhou, J.N. Beltramini, Y.X. Fan, G.Q. Lu, *Chem. Soc. Rev.*, 2008, **39**, 527-549.
- B. Katryniok, H. Kimura, P. Fongarland, F. Dumeignil, *Green Chem.*, 2011, **13**, 1960-1979.
- D. Sun, Y. Yamada, S. Sato, W. Ueda, *Green Chem.*, 2017, **19**, 3186-3213.
- A. Behr, J. Eilting, K. Irawadi, J. Leschinski, F. Lindner, *Green Chem.*, 2008, **10**, 13-30.
- D. Sun, Y. Yamada, S. Sato, W. Ueda, *Appl. Catal. B: Environ.* 2016, **193**, 75-92.
- M.H. Haider, N.F. Dummer, D.W. Knight, R.L. Jenkins, M. Howard, J. Moulijn, S.H. Taylor, G.J. Hutchings, *Nat. Chem.* 2015, **7**, 1028-1032.
- A.P. And, P. Tundo, *Ind. Eng. Chem. Res.* 2005, **44**, 8535-8537.
- E.V. Ryneveld, A.S. Mahomed, P.S.V. Heerden, M.J. Green, H.B. Friedrich, *Green Chem.*, 2011, **13**, 1819-1827.
- M.L. Shoji, V. Dasireddy, S. Singh, D.J. Morgan, H.B. Friedrich, *ACS Sustain. Chem. Eng.*, 2016, **4**, 5752-5760.
- X.F. Lin, Y.H. Lv, Y.Y. Xi, Y.Y. Qu, C.G. Liu, *Energy Fuels*, 2014, **28**, 3345-3351.
- Y. Nakagawa, K. Tomishige, *Catal. Sci. Technol.*, 2011, **1**, 179-190.
- S.Y. Yang, D.S. Park, J. Yi, *Catal. Sci. Technol.*, 2014, **4**, 3191-3202.
- S. Xia, R. Nie, X. Lu, L. Wang, P. Chen, Z. Hou, *J. Catal.*, 2012, **296**, 1-11.
- S. Zhu, Y.L. Zhu, S.L. Hao, H.Y. Zheng, Y.W. Li, *Green Chem.*, 2012, **14**, 2607-2616.
- L. Zheng, H. Zhao, J. Fu, X. Lu, Z. Hou, *Appl. Clay Sci.*, 2018, **153**, 54-60.
- S.L. James, *Chem. Soc. Rev.*, 2003, **32**, 276-288.

- 23 M. Eddaoudi, J. Kim, N. Rosi, D. Vodak, J. Wachter, M. O'Keeffe, O.M. Yaghi, *Science*, 2002, **295**, 469-472.
- 24 S. Dang, Q.-L. Zhu, Q. Xu, *Nat. Rev. Mater.*, 2017, **3**, 17075-17088.
- 25 W. Xia, A. Mahmood, R. Zou, Q. Xu, *Energy Environ. Sci.*, 2015, **8**, 1837-1866.
- 26 L. Zheng, X. Li, W. Du, D. Shi, W. Ning, X. Lu, Z. Hou, *Appl. Catal. B: Environ.*, 2017, **203**, 146-153.
- 27 G. Huang, Q. Li, D. Yin, L. Wang, *Adv. Funct. Mater.*, 2017, **27**, 1604941-1604947.
- 28 W. Du, L. Zheng, X. Li, J. Fu, X. Lu, Z. Hou, *Appl. Clay. Sci.*, 2016, **123**, 166-172.
- 29 X. Wang, F. Li, W. Li, W. Gao, Y. Tang, R. Li, *J. Mater. Chem. A*, 2017, **5**, 17982-17989.
- 30 L. Yang, L. Yu, M. Sun, C. Gao, *Catal. Commun.*, 2014, **54**, 86-90.
- 31 Y. Lü, W. Zhan, Y. He, Y. Wang, X. Kong, Q. Kuang, Z. Xie, L. Zheng, *ACS Appl. Mater. Inter.*, 2014, **6**, 4186-4195.
- 32 M. Haneda, Y. Kintaichi, N. Bion, H. Hamada, *Appl. Catal. B: Environ.*, 2003, **46**, 473-482.
- 33 C.W. Tang, C.B. Wang, S.H. Chien, *Thermochim. Acta.*, 2008, **473**, 68-73.
- 34 N.N. Madikizela-Mnqanqeni, N.J. Coville, *J. Mol. Catal. A Chem.*, 2005, **225**, 137-142.
- 35 B.J. Tan, K.J. Klabunde, P.M.A. Sherwood, *J. Am. Chem. Soc.*, 1991, **113**, 855-861.
- 36 N.S. Mcintyre, D.D. Johnston, L.L. Coatsworth, R.D. Davidson, J.R. Brown, *Surf. Interface. Anal.*, 1990, **15**, 265-272.
- 37 L. Formaro, R. Giannantonio, C. Pastorelli, R. Carli, *J. Phys. Chem.*, 1992, **96**, 3197-3200.
- 38 J. Cheng, Y. Lu, K. Qiu, H. Yan, X. Hou, J. Xu, L. Han, X. Liu, J.-K. Kim, Y. Luo, *Phys. Chem. Chem. Phys.*, 2015, **17**, 17016-17022.
- 39 E.C. Onyiriuka, *J. Non-Cryst. Solids.*, 1993, **163**, 268-273.
- 40 I. Melián-Cabrera, M.L. Granados, J.L.G. Fierro, *J. Catal.*, 2002, **210**, 285-294.
- 41 E. S. Vasiliadou and A. A. Lemonidou, *Chem. Eng. J.*, 2013, **231**, 103-112.
- 42 E. van Ryneveld, A.S. Mahomed, P.S. van Heerden, M.J. Green, C. Holzappel, H.B. Friedrich, *Catal. Sci. Technol.*, 2014, **4**, 832-837.
- 43 R. Mane, S. Patil, M. Shirai, S. Rayalu, C. Rode, *Appl. Catal. B: Environ.*, 2017, **204**, 134-146.

Graphical abstract

CoZn-ZIF derived ZnCo₂O₄-framework for the synthesis of alcohols from glycerol

Huaiyuan Zhao, Yuanyuan Jiang, Ping Chen, Jie Fu, Xiuyang Lu, Zhaoyin Hou

A novel Co/ZnO catalyst obtained from CoZn-ZIF precursor is highly active and selective for the synthesis of ethanol from glycerol.

